Electronic Supplementary Material (ESI) for Journal of Materials Chemistry A.

Electronic Supplementary Information

N-type cathode interlayer based on dicyanomethylenated quinacridone derivative for high-performance polymer solar cells

Weiping Chen, Junjie Lv, Jianxiong Han, Youchun Chen, Tao Jia, Fenghong Li* and Yue Wang*

State Key Laboratory of Supramolecular Structure and Materials, Jilin University, Changchun, Qianjin Avenue, 130012, P. R. China. E-mails: fhli@jlu.edu.cn (F. Li); yuewang@jlu.edu.cn (Y. Wang).

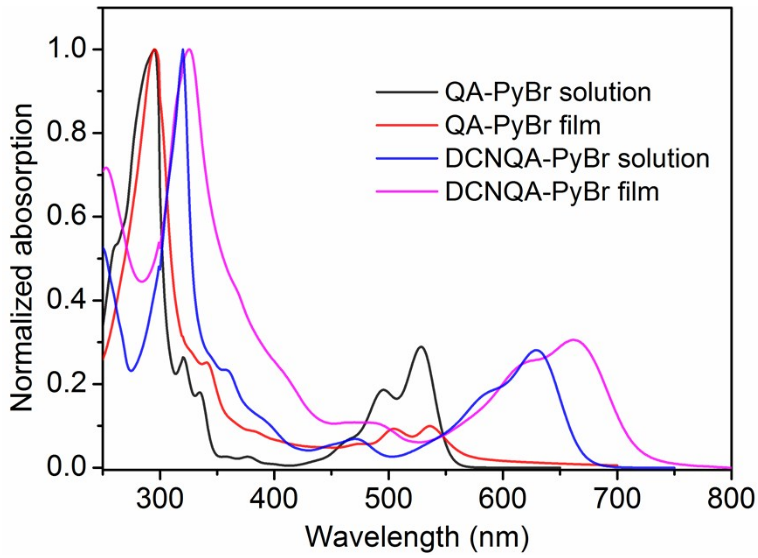

Fig. S1. Normalized UV-vis absorption spectra of QA-PyBr and DCNQA-PyBr in dilute solutions (1×10^{-5} M in DMF) and in thin films.

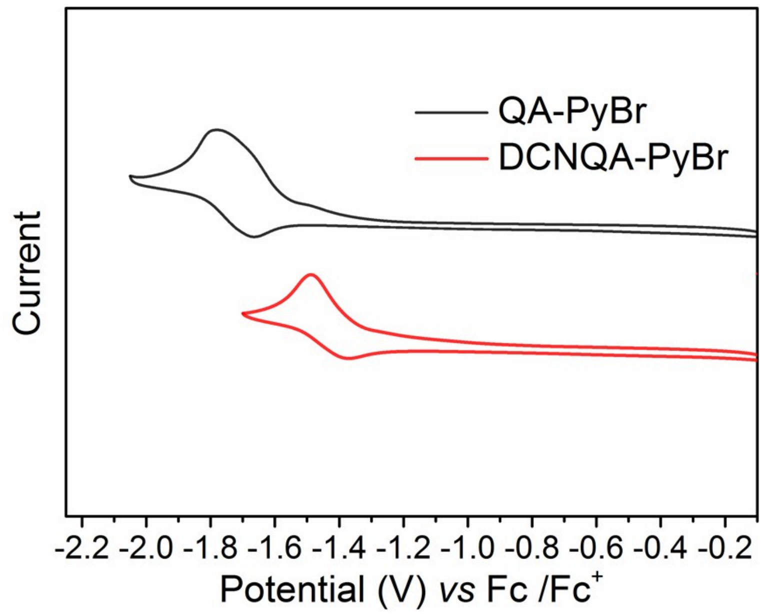

Fig. S2. Cyclic voltammograms of QA-PyBr and DCNQA-PyBr measured in DMF.

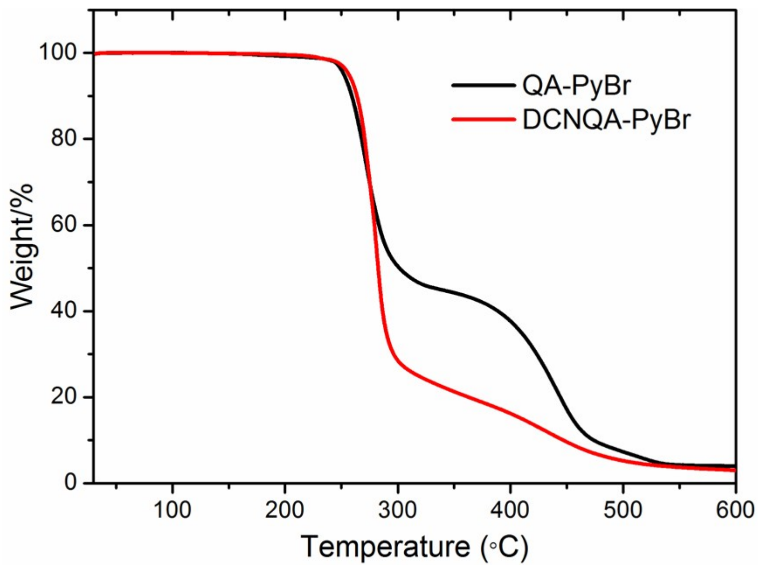

Fig. S3. TGA curves of QA-PyBr and DCNQA-PyBr.

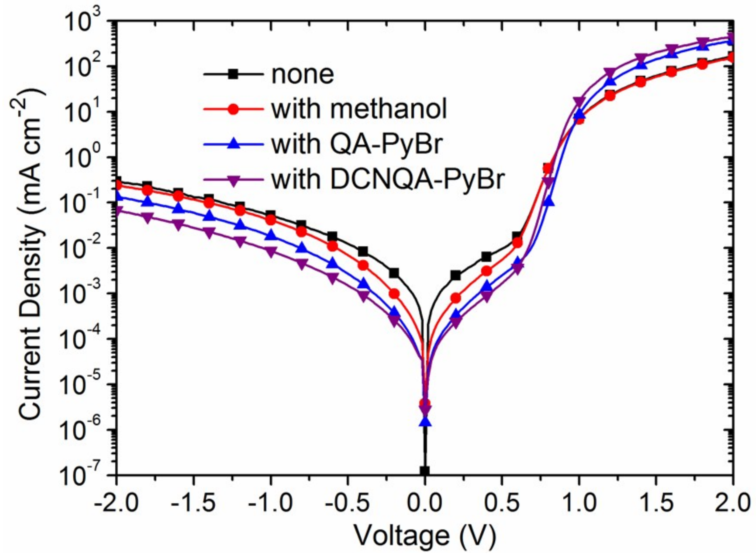

Fig. S4. *J-V* curves of the QA-PyBr, DCNQA-PyBr incorporated, methanol-treated, and Al-only devices under dark.

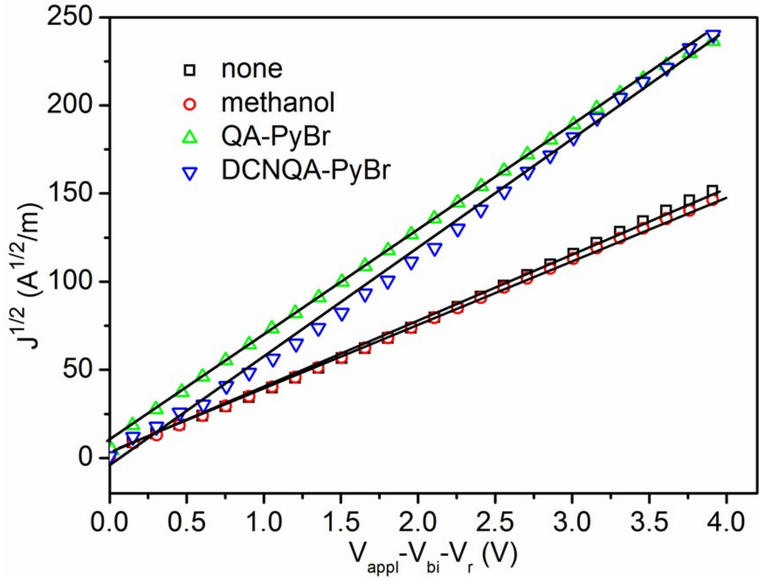

Fig. S5. $J^{1/2}$-V characteristics of the electron-only devices.

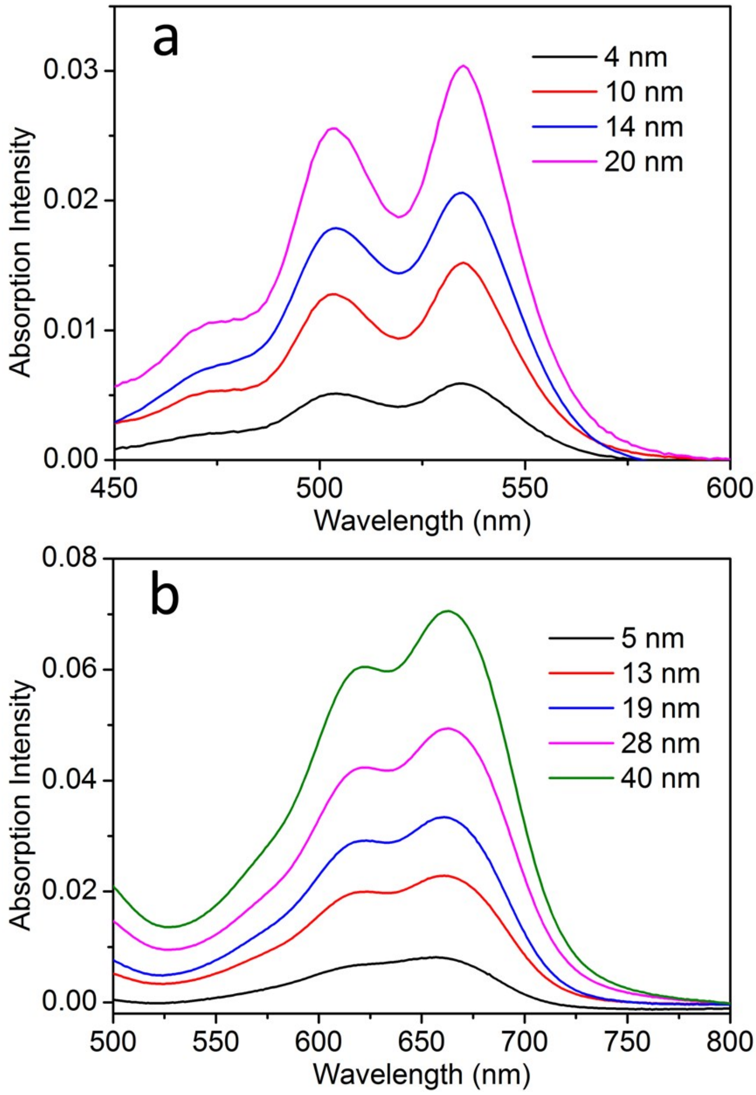

Fig. S6. The absorption spectra of (a) QA-PyBr films and (b) DCNQA-PyBr films with different thickness on the quartz substrates. The thickness of 20 nm for QA-PyBr film and 40 nm for DCNQA-PyBr film were determined by the profilometer.

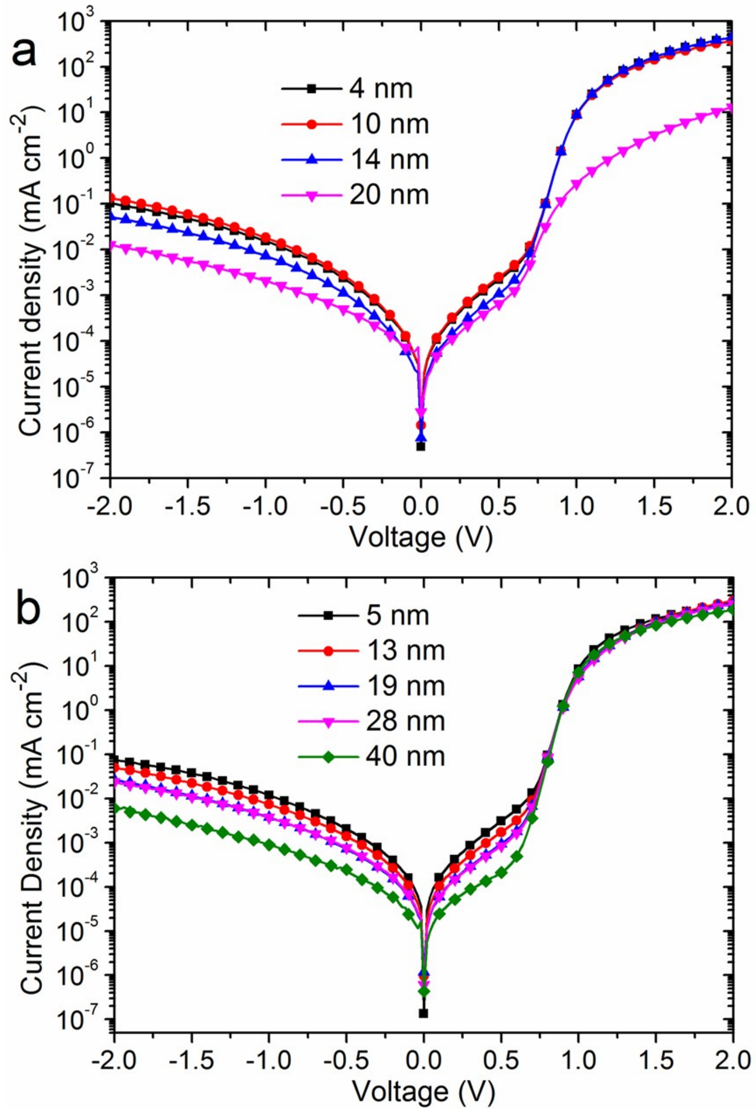

Fig. S7. *J-V* characteristics of the devices with various thicknesses of QA-PyBr (a) and DCNQA-PyBr (b) interlayer under dark.

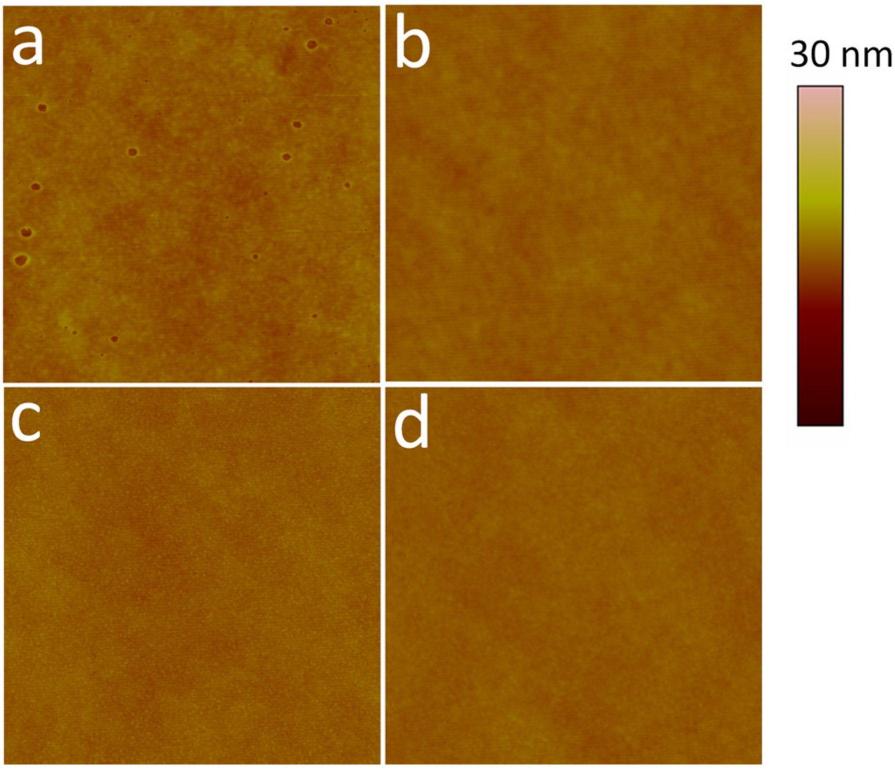

Fig. S8. Atomic force microscopy (AFM) images (5 × 5 μm) of with various thicknesses QA-PyBr interlayers atop of the PCDTBT:$PC_{71}BM$ layer. (a) 4 nm, RMS: 0.57 nm; (b) 10 nm, RMS: 0.34 nm; (c) 14 nm, RMS: 0.46 nm; (d) 20 nm, RMS: 0.30 nm.

Table S1. Photophysical data, cyclic voltammetric data and HOMO/LUMO energy levels.

	λ_{onset} (nm)[a]	E_g^{opt} (eV)[b]	E_{re}^{onset} (V)[c]	LUMO (eV)[d]	HOMO (eV)[e]
QA-PyBr	553	2.24	-1.58	–3.22	-5.46
DCNQA-PyBr	685	1.81	-1.35	–3.45	-5.26

[a] The lowest-energy absorption edge of the absorption spectra. [b] Optical band gap estimated from the lowest-energy absorption edge. [c] Onset reduction potential (*vs.* ferrocene/ferrocenium) measured in DMF. [d] Deduced from the onset reduction potentials, assuming that the energy level of ferrocene lies 4.8 eV below the vacuum level. $E_{LUMO} = -(E_{re}^{onset} + 4.80)$ eV. [e] Calculated from LUMO and E_g^{opt}. $E_{HOMO} = (E_{HOMO} – E_g^{opt})$ eV.

Table S2. The measured J_{sc} values (from the J-V curves) and calculated J_{sc} values (from the EQE spectra) of the PCDTBT:$PC_{71}BM$ devices under 100 mW cm^{-2} AM 1.5G irradiation.

	none	LiF	methanol	QA-PyBr	DCNQA-PyBr
Measured J_{sc} (mA cm^{-2})	10.24	10.64	10.30	11.19	11.33
Calculated J_{sc} (mA cm^{-2})	10.07	10.51	10.12	10.80	11.00

Table S3. The measured J_{sc} values (from the J-V curves) and calculated J_{sc} values (from the EQE spectra) of the P3HT:$PC_{61}BM$ devices under 100 mW cm^{-2} AM 1.5G irradiation.

	none	LiF	DCNQA-PyBr
Measured J_{sc} (mA cm^{-2})	9.12	10.13	10.25
Calculated J_{sc} (mA cm^{-2})	9.06	10.00	10.15

Table S4. The measured J_{sc} values (from the J-V curves) and calculated J_{sc} values (from the EQE spectra) of the PTBT:$PC_{71}BM$ devices under 100 mW cm^{-2} AM 1.5G irradiation.

	none	LiF	DCNQA-PyBr
Measured J_{sc} (mA cm^{-2})	14.62	15.19	16.51
Calculated J_{sc} (mA cm^{-2})	14.48	15.07	16.20